Large-eddy simulation and experimental study of a partially premixed hydrogen / air swirled burner: impact of the injection system

Karine Truffin, Paul-Georgian Luca, Tran Ngoc Duc Ho, Justin Bertsch, Giampaolo Maio, Cedric Mehl, Victor Coquin, Gilles Cabot, Bruno Renou, Lucio Taddeo

Large-eddy simulation and experimental study of a partially premixed hydrogen / air swirled burner: impact of the injection system

Karine Truffin[*], Paul-Georgian Luca[*], Tran Ngoc Duc Ho[*], Justin Bertsch*, Giampaolo Maio*, Cedric Mehl[*], Victor Coquin[,***], Gilles Cabot[**], Bruno Renou[**], Lucio Taddeo[***]**
karine.truffin@ifpen.fr
[*]IFP Energies Nouvelles, Institut Carnot IFPEN Transports Energie, 1-4 Av. du Bois Préau, 92852 Rueil-Malmaison, France
[**]UNIROUEN, INSA Rouen, CNRS, CORIA, Normandie University, 76000 Rouen, France
[***]CETIAT, 25 Avenue des Arts, 69100 Villeurbanne

Abstract

Hydrogen-powered combustion devices (boilers, burners) and associated equipment (ignition and flame detection devices, gaskets, etc.) will have to comply with the same safety requirements, energy performance and pollutant emission thresholds as those set by regulations applicable to appliances fuelled by natural gas. Hydrogen combustion however suffers from flame stability and flashback issues, due to its large flame speed and low minimum ignition energy. This makes the use of hydrogen more challenging than natural gas. This study follows previous works dedicated to premixed H_2/CH_4/air combustion in swirled and/or bluff-body flows, where the main difficulty concerns flashback, which often limits the mass quantity of hydrogen substituted for methane.

To control flashback, two solutions are considered. The first is to operate in a non-premixed flame regime, but this solution generates the largest NO emissions. Nevertheless, it guarantees the prevention of flashbacks. The second solution is to operate in a partially premixed regime. Here, the goal is to achieve optimal mixing between the fuel and air in a very short time and at the smallest distance. If this mixing condition is met, the combustion will produce minimal nitrogen monoxide (NOx) akin to fully premixed combustion, with the benefit of avoiding any flashback.

The objective of this study is to assess the impact of the hydrogen-air mixture quality in a swirled bluff-body burner with modifiable injection geometry, on the topology of the stabilized flames as well as on pollutant formation. Comparisons of results from large-eddy simulations with measurements allow to validate the results, in terms of aerodynamic field, flame shape and position. Further analysis of the LES results show that the centripetal injection yields a more uniform air/hydrogen mixture. This also leads to a reduction in the maximum temperature, subsequently contributing to lower emissions of NOx.

Introduction

The use of hydrogen as a fuel is a particularly interesting way to produce heat directly (process engineering) or indirectly (individual or collective boilers), which still requires many research efforts for large-scale deployment. However, the combustion characteristics are strongly modified: higher temperature and flame speed, reduction of the ignition energy by an order of magnitude, extension of the flammability range, modification of the emission spectrum (UV range). All these aspects make its use in the industry more challenging. At the same time, the significant reduction in the quenching distance, i.e., the minimum distance between the flame front and the wall, can cause the appearance of potentially harmful phenomena for the burner: premature deterioration accentuated by the high-water vapor content of the burned gases, appearance of hot spots and increased risk of flashback. The high diffusivity of hydrogen is also an essential point to consider because, beyond the associated safety problems, it implies a strong decrease of the Lewis number, which expresses the relative importance of species diffusion compared to heat diffusion. For hydrogen, the faster mass diffusion tends to increase the thermo-diffusive instabilities, compared to hydrocarbon flames. Finally, the production of nitrogen oxides has to be subject of a particular attention because the control of this pollutant is essential to perpetuate the use of hydrogen burners.

Several experimental studies have explored the impact of adding hydrogen to methane burners. In a 3kW swirled burner study by Choi et al. (Choi et al., 2021), the hydrogen concentration was varied from 0 to 50% (volume) at an intermediate scale between research burners and industrial/aeronautical applications. The results demonstrated that the addition of hydrogen had a stabilizing effect on the flame. This effect was accompanied by an increase in flame temperature and a reduction in flame size. Similar effects were observed in a swirled burner study in (Schefer, Wicksall and Agrawal, 2002). These changes can be attributed, in part, to the significantly higher laminar flame speed of hydrogen compared to methane, and higher resistance to strain (Guiberti et al., 2015). Acoustic forcing experiments were conducted on a swirled methane burner with added hydrogen using different injection configurations, as reported in (Schuller et al., 2022). It was observed that in the premixed configuration, the flame size decreased, aligning with previous findings (Choi et al., 2021; Schefer, Wicksall and Agrawal, 2002). However, the range of frequencies at which the flame responded to external forcing expanded with increasing hydrogen concentration. In contrast, when hydrogen was used as a pilot flame at the burner base, the sensitivity range decreased as hydrogen concentration increased. The heat released by the pilot flame counteracted disturbances downstream in the flow. Furthermore, there have been attempts to adapt methane burners into 100% hydrogen burners, but their adoption remains limited due to safety concerns, particularly regarding flashback. An example of such an adaptation are the methane gas turbine burner in (Cappelletti and Martelli, 2017) and the Preccinsta premixed burner from DLR-Stuttgart (Chterev and Boxx, 2021), which were transformed into a pure premixed hydrogen configuration to study flashback limits and NOx production. Recently the HYLON burner (Marragou et al., 2023a), featuring an innovative dual swirl coaxial injector, has recently been designed specifically for operating with an H_2/Air mixture in gas turbines.

CFD is a recognized tool that can help the retrofitting process giving access to a high-fidelity 3D representation of the investigated technological configurations. A few recent numerical studies on hydrogen combustion in swirl stabilized burned can be found. In a recent paper (Schmidt et al., 2023), combined numerical and experimental studies of a partially premixed hydrogen burner were performed to improve the mixture formation by geometric optimization of the injection system. Large-eddy simulations (LES) of a steam-diluted H2 flame was studied in (Palulli et al., 2023) with a gas turbine combustor composed of two swirlers. The fuel entered the first swirler through radial and axial holes. In (Aniello et al., 2023) a lifted V-flame and an anchored one were studied for a global equivalence ratio of 0.45. LES allowed to analyse in detail the flame structures. In (Marragou et al., 2023b), a comprehensive numerical study of the HYLON burner and strategy was proposed to predict the flame stabilization (lifted or anchored to the injector).

The objective of this study is to assess the impact of the hydrogen-air mixture quality in a swirled bluff-body burner with modifiable injection geometry, on the topology of the stabilized flames as well as on pollutant formation. The HyCoP burner, experimentally investigated at CORIA laboratory is selected to that purpose and two injection systems are investigated. Comparisons of results from large-eddy simulations with measurements allow to validate the results, in terms of aerodynamic field, flame shape and position and to quantify NOx emissions.

Experimental setup: the HYCOP swirled partially premixed burner

The CORIA HyCOP burner selected for this work is described in Figure **1**. It consists of an intake plenum at the bottom and a rectangular combustion chamber with four optical accesses for the different optical diagnostics. A cone-shaped exhaust plenum is placed at the outlet of the combustion chamber to limit air re-entry from the environment. The dimensions of the injection system are not shown for reasons of confidentiality.

The intake system consists of a swirler associated with a premixing chamber featuring a centrally positioned bluff body. The premixing chamber has an internal diameter of 18 mm and a length of 30 mm. Once the airflow has been evenly distributed and homogenized in the plenum, it passes through the swirler to enter the premixing chamber. Hydrogen is introduced into the premixing chamber at a distance L_2 upstream from the swirler, enabling the two gases to mix along a length of L_1 before entering the combustion chamber. The ratio of diameters between the outer and inner tubes (in black) r_2/r_1 is fixed.

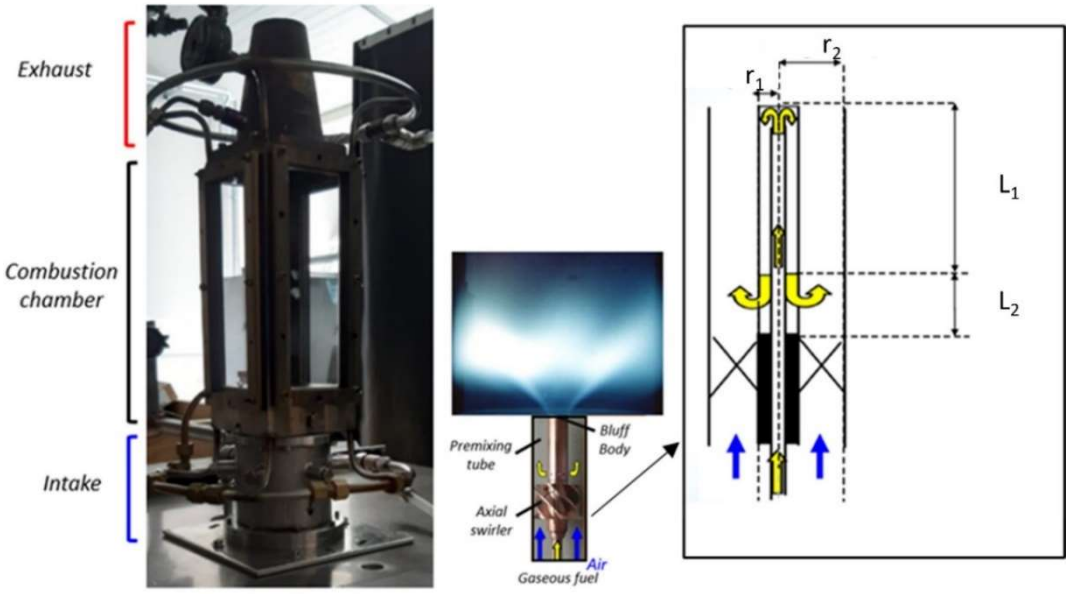

Figure 1. The HyCoP burner: (left) experimental test-rig; (right) air/fuel centrifugal injection.

Two injection systems are studied. The principle is shown in Figure 2. Hydrogen injection is carried out using the multi-transversal jet technique in a cross-swirled airflow. The radial direction in which the fuel flow exits the holes determines the two configurations under the scope of this study. If the fuel flows outwards to mix with air, it is called "centrifugal" injection while if it flows inwards, the injection is called "centripetal". In the centrifugal configuration, hydrogen is injected through n holes of diameter d positioned on the bluff body toward the outer edge. In the centripetal configuration, hydrogen is injected through similar holes located on the external part of the premixing tube towards the bluff body.

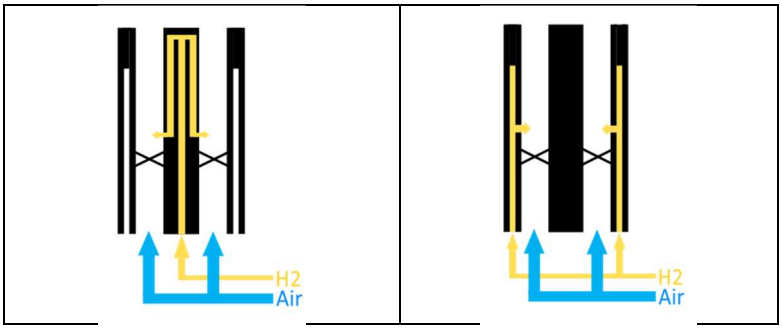

Figure 2. Two investigated hydrogen injection systems: (left) centrifugal injector; (right) centripetal injector.

The partially premixed flow enters in the combustion chamber, where the flame is stabilized by the swirled flow and the bluff-body. The study focuses on achieving a power output of 14.87 kW, maintaining a global equivalence ratio of 0.769, and an air injection speed of approximately 30 m/s. Further details regarding the various injection operations are provided in Table 1.

Table 1. Flame parameters of the experimental cases

Thermal Power [kW]	14.87	
Inlet temperature [K]	300	
Equivalence ratio [-]	0.769	
Case	Centrifugal 100 % H_2	Centripetal 100 % H_2
Air flow rate [g/s]	5.556	
Fuel flow rate [g/s]	0.124	

Particle image velocimetry (PIV) is used to measure 2D velocity and the flow topology in the combustion chamber. The flow is seeded with micronical Zirconium Oxide (ZrO2) particles which are illuminated by a Quatronix Dual-Darwin-80 laser with an acquisition frequency of 5 kHz and a delay time

of 10 µs between each image. Particles images are recorded by a high-speed camera Phantom V-2512 with an acquisition frequency of 10 kHz. This camera is equipped with a macro lens Zeiss Makro-Planar (f=100 mm) and an interference filter centred to 528 nm to suppress flame chemiluminescence. Planar laser-induced fluorescence (PLIF) on OH radical is used to characterize the local flame structure. The fluorescence signal is induced by a laser sheet tuned to the appropriate wavelength for work with the Q1(5)(1-0) transition. This signal is collected by intensified camera PI-MAX 4 (emICCD) equipped with a UV-Cerco lens (f=100 nm) and an Asahispectra 313±10 nm filter (XHQA313).

Numerical setup and models

Large-eddy simulation

In the present article the simulations are performed with the CONVERGE-CFD 3.0 solver (Richards, Senecal and Pomraning, 2022) co-developed by IFPEN. It features a second order centred finite volume spatial discretization and second-order Crank-Nicolson time discretization. The numerical solver uses the compressible pressure-based PISO algorithm for the treatment of pressure-velocity coupling. The species diffusivities are computed using a mixture-average approach. Each species has its own mass diffusivity which depends on temperature. Therefore, the Lewis number is different for each species and varies through the flame front. The Soret and Dufour effects are neglected. Detailed chemical kinetics are solved using the CVODE solver. The adoption of a global mechanism in this configuration poses challenges, as it exhibits lower accuracy in predicting NOx emission and it necessitates providing appropriate functions for pre-exponential factors for the whole range of equivalence ratios. In the current study, the GRI-Mech 3.0 mechanism is employed to described H_2/air chemistry, but the carbon-containing portion is eliminated, resulting in a modified GRI-Mech with 70 reactions and 19 species.

For turbulent flows, subgrid stresses are modelled using the Sigma model (Baya Toda et al., 2014; Nicoud et al., 2011). The flame/turbulence interaction is modelled by the Thickened Flame Model (Colin et al., 2000). This model artificially increases the thickness of the flame by a factor denoted as F, and it incorporates the influence of subgrid-scale (SGS) structures through the application of an efficiency factor E, as described in (Charlette et al., 2002). In the current study, we adopt a dynamic formulation of TFM, following the approach presented by (Legier et al., 2000). It is worth noting that this thickening process is confined to the flame region, defined by a flame sensor function detecting the heat release rate (Jaravel, 2016) denoted as "S," where S equals 1. Furthermore, our focus is specifically on the TFM-AMR extension, which was proposed in (Mehl et al., 2021; Mehl et al., 2018). This extension employs adaptive mesh refinement (AMR) to accurately resolve the flame front when S is greater than zero.

Boundary conditions

The geometry of the computational domain in shown in Figure 3 (a). The intake plenum and air swirl injector are incorporated in the numerical domain. The exhaust plenum represents the surrounding atmosphere. The longitudinal axis corresponding to the mean flow direction aligns with the z-axis. The z=0 plane is located at the end of the mixing tube. The chamber is 23 cm long and 10 cm wide.

To maintain a sufficient distance from the turbulent flow and vortical structures originating from the combustion chamber, the outlet boundary condition is placed far downstream (Figure 3 (b)). Wall shear stress and wall heat fluxes are modelled using the classical law-of-the-wall. In non-reactive cases, adiabatic wall conditions are applied, while in reactive cases, isothermal wall conditions are imposed. The temperature conditions at the walls can be determined based on experimental measurements, a Conjugate Heat Transfer (CHT) coupling method in (Agostinelli et al., 2022), or optimization procedures that are computationally expensive, as in (Benard et al., 2019). As there are no available experimental temperature measurements, constant temperature values are enforced in the combustion chamber, relying on previous studies (Benard et al., 2019) and the expertise of the researchers (see Figure 3 (c)). A CHT coupling will be considered in the future.

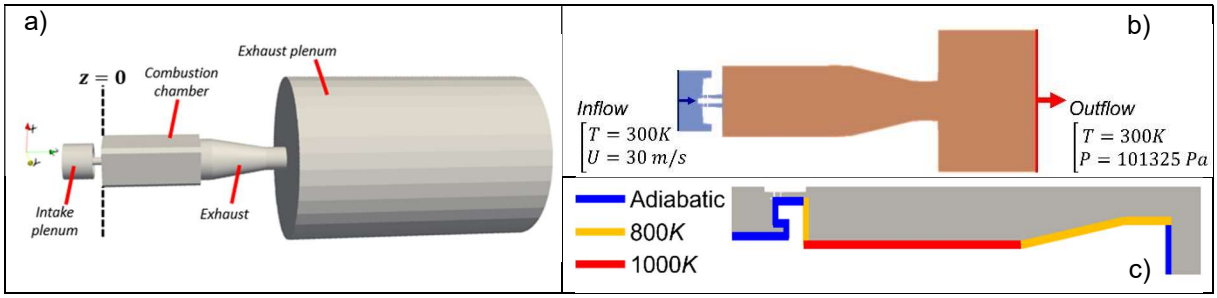

Figure 3. Computational domain: (a) global view; (b): inflow/outflow boundaries; (c) thermal conditions along wall boundaries of the burner and combustion chamber.

Meshing strategy

CONVERGE-CFD features a cut-cell Cartesian technique to mesh complex geometries and handle intricate shapes at the boundaries. The base grid size (BGS), which represents the length of the base cubic cell, remains consistent across all simulations, regardless of variations in geometry and setup conditions. In this study, the BGS is set to 4 mm. Additionally, CONVERGE offers a convenient approach for implementing static mesh refinements within the simulated domain, known as "embeddings." The desired grid size (GS) for an "embedded" region can then be defined as $GS = BGS/2^n$ with n being the desired refinement level for each individual embedding. The mesh sensitivity study for the cold flow simulations involves the use of three different meshes, as illustrated in Figure 4: a coarse mesh (CM), an intermediate one (IM) and a fine mesh (FM). Transitioning from (a) to (b) in Figure 4, modifications to both the Base Grid Size (BGS) and the refinement levels are applied. In contrast, the transition from mesh (a) to (c) only entails adjustments to the refinement levels n. To capture the primary jet at the swirler exit while minimizing computational costs, progressive trapezoidal refinements are employed. An *a posteriori* analysis of the velocity fields on the finest mesh shows that the maximum turbulent to laminar viscosity ratio reaches 14 in the swirler and about 5 in the premixing chamber and at the burner exit, which is a first indicator of the mesh quality. The normalized wall distance y+ reaches a maximum value close to 20 in the swirler, which is also consistent with the use of a law-of-the-wall approach, with a linear profile for y+ < 13 and a logarithmic profile for y+ > 13. Fore reactive simulations, the mesh is refined in the premixing chamber down to 125 microns to achieve a minimum of 10 cells across each fuel injection hole. In addition, a fixed AMR refinement level is set to 5, and the number of grid points through the flame front, denoted as n_{res} is set at 10. This configuration ensures that the value of the target thickening factor satisfying the condition $\mathcal{F}_t\delta_l^0 = n_{res}\Delta_x^{flame}$, never exceeds 4. δ_l^0represents the laminar flame thickness and is determined as a function of the local thermodynamic conditions.

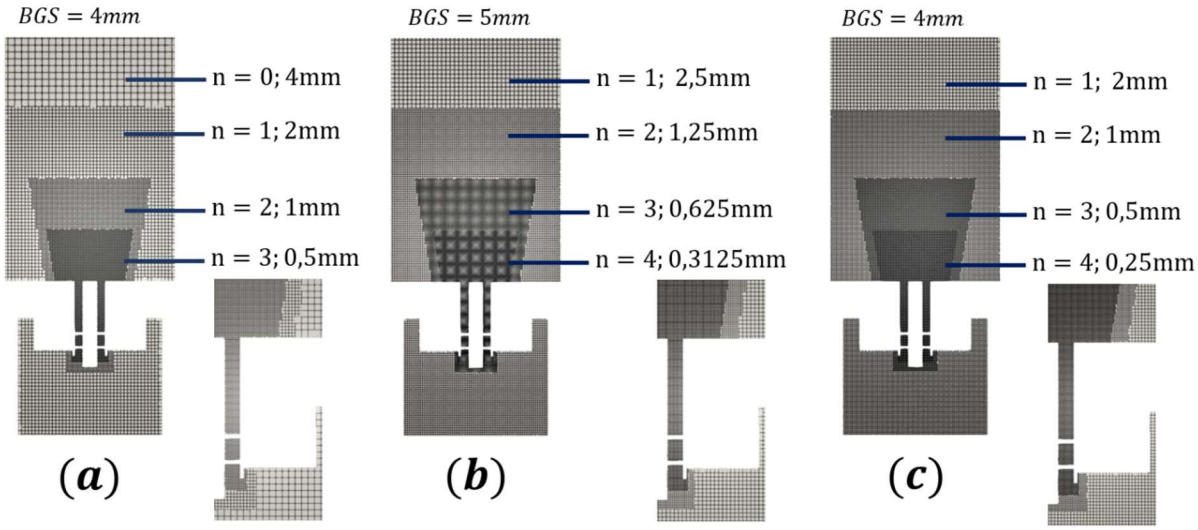

Figure 4. Mesh resolution in the swirler and in the combustion chamber. Central longitudinal cut showing (a) the coarse mesh CM (0.9M cells); (b) the intermediate mesh IM (3.6 M cells); (c) the fine mesh FM (7 M cells).

Nonreactive flow

A convective time (t_{conv}) has been defined to assess the evacuation time of the initial condition and determine statistical convergence. This parameter represents the time required for an imaginary fluid particle to cross the entire domain of length L=0.45m (combustion chamber and convergent exhaust), with a chosen characteristic velocity of 2.5 m/s, which corresponds to the axial velocity in the convergent exhaust under the cold configuration, with an air flow rate of 6.588 g/s. The calculated convective time is t_{conv}=0.18 s. To ensure reliable statistical convergence, the duration over which statistics are collected should ideally exceed t_{conv} after an initial stabilization period.

Once the flow has stabilized for a duration equal to or greater than $5t_{conv}$, irrespective of the mesh size, statistics are collected until convergence is observed. In Figure 5, a comparison is made between the mean axial velocity and experimental Root Mean Square (RMS) fields obtained from Particle Image Velocimetry (PIV) and the results from simulations conducted using the three different mesh configurations on the same X-Z plane section. Due to the axisymmetric geometry, only the left side of the experimental jet is considered as a reference, and the simulation results also focus on the left-hand side. An offset of 2 mm is present in the experimental PIV measurements, which is represented as a greyed zone indicating the absence of measurement data. The general jet structure is maintained in the simulations regardless of mesh size, although the jet angle is slightly underpredicted for the less refined meshes (a) and (b). Resolved RMS velocities obtained with IM and FM show variations closer to the experimental measurements compared to CM. This improvement can be attributed to the fact that a finer mesh resolves more turbulence scales allowing for better representation of fluctuations.

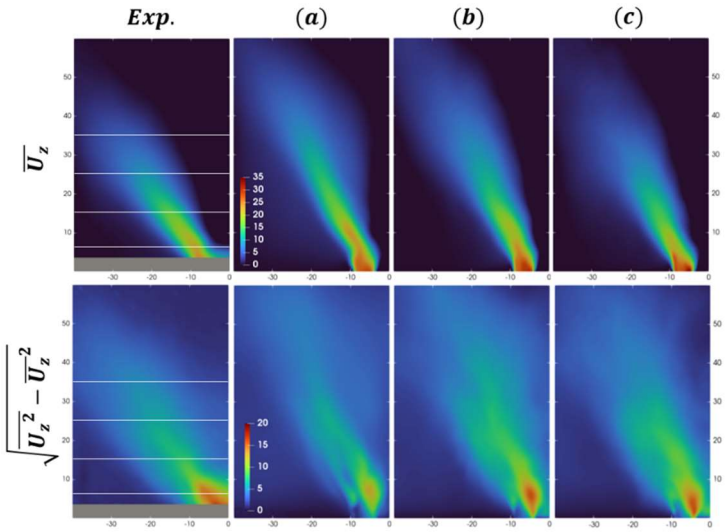

Figure 5. Half fields of axial velocity averaged over the (X, Z) plane and corresponding RMS ($m.s^{-1}$) - Experimental field with positioning of the extracted profiles, (a) CM, (b) IM, (c) FM - axes in (mm).

To provide quantitative comparisons, radial profiles are extracted at z = 5, 15, 25, and 35 mm (Figure 6). Given the axial symmetry of the jet, orthonormal averages are numerically obtained in the (X, Z) and (Y, Z) planes. Near the swirler outlet (z = 5 mm), little difference is observed between the three meshes in the axial velocity field. However, at z = 15 mm and z = 25mm, the refined mesh results in a more open field that closely matches the experimental data. At z = 25 mm, the refined mesh aligns almost perfectly with the measurements, while CM and IM overestimate the axial velocity, which is noticeable at z = 15, 25, and 35 mm, as previously observed in the 2D fields in Figure 5.The RMS profiles of the axial velocity at z = 5mm vividly demonstrate the impact of mesh resolution on turbulent scales. It is expected that with a refined mesh, the RMS values increase, closely matching the experimental profile. This trend becomes smoother as we move away from the swirler. Table 2 presents the relative difference in mean axial velocity and RMS of axial velocity between meshes FM and IM, as well as between meshes FM and CM. These differences have been computed by considering the velocity statistics averaged over each radial profile for several axial positions Z. A noticeable reduction of the error by a factor 2 in average is observed from CM to IM, except for the rms value at z = 35 mm. This reduction is slightly higher than the mesh size ratio between IM and CM equal to 1.6. In conclusion, the FM appears to be the most

suitable choice for obtaining results that closely resemble the measurements and will be employed in the reactive case.

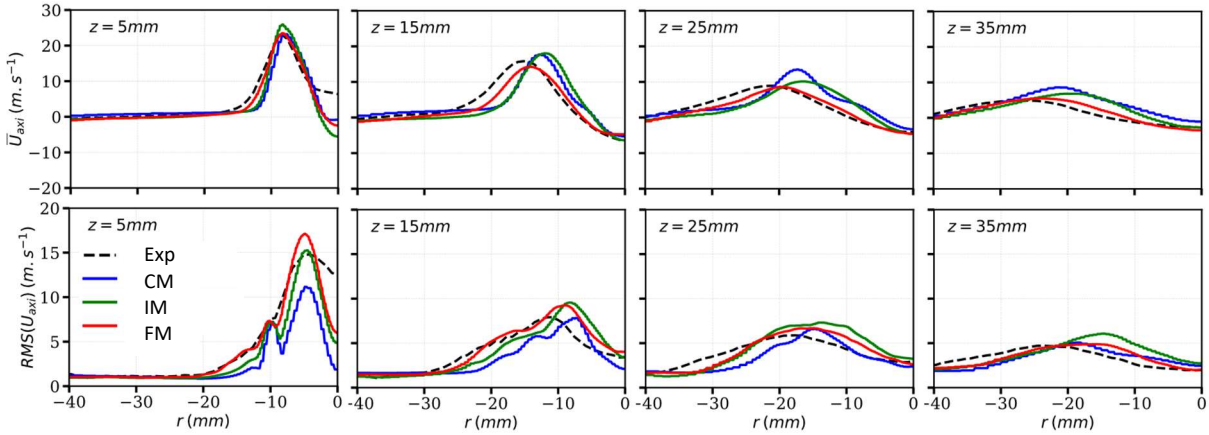

Figure 6. Radial profiles of the axial velocity and the corresponding RMS.

	Z = 5mm		Z = 15mm		Z = 25mm		Z = 35mm	
	(FM-IM) / FM (%)	(FM-CM) / FM (%)	(FM-IM) / FM (%)	(FM-CM) / FM (%)	(FM-IM) / FM (%)	(FM-CM) / FM (%)	(FM-IM) / FM (%)	(FM-CM) / FM (%)
U_{ax}	5.7	11	22	49	48	100	80	165
$RMS(U_{ax})$	15	32	6.6	20	6	15	11	5

Table 2. Relative differences in mean axial velocity and in its RMS obtained from several radial profiles between FM and IM or CM meshes.

Reactive flows

Instantaneous fields

Regarding the flame topology, Figure 7 shows the flame front at distinct independent instants for the two cases. The flame front is identified by a temperature iso-surface (400 K) and is coloured by the instantaneous axial velocity. Theses snapshots unveil compact flames, particularly noticeable with the centripetal injector (≤ 5 cm length), located close to the burner inlet. The flapping of the flame front generates pockets of fresh gas that are released in the combustion chamber. A reduced flow velocity is observed at the outer periphery of the burner inlet with the centrifugal injection, contrasting with the centripetal one, which will be explained further.

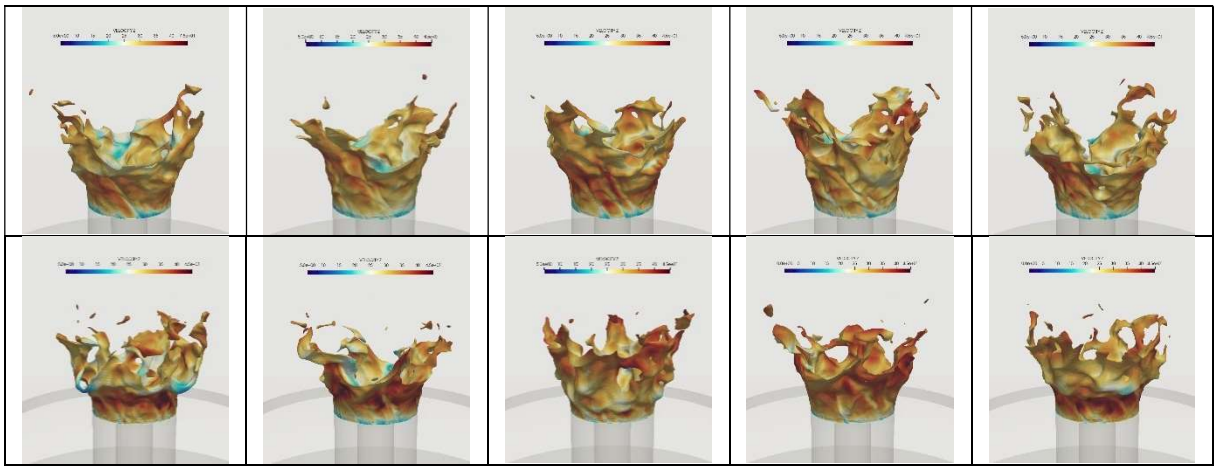

Figure 7. Instantaneous fields from LES showing an iso-surface of the temperature (400 K) coloured by the axial velocity (colormap from 5 to 45 m/s). Top: centrifugal; bottom: centripetal.

Impact on the mixing

To assess the mixing quality, the average equivalence ratio in the (X, Y) plane for the two injection methods is shown in Figure 8. In qualitative terms, the cooler colours displayed in the centripetal case indicate a globally leaner mixture, with a reduction in isolated fuel-rich zones in the mixing tube, which are more prevalent in the centrifugal injector. The position of higher hydrogen concentration has notably shifted to the outer rims of the mixing tube in the centripetal case. In this region, the higher velocity values may enhance the mixing. The normalized probability density functions (PDF) of the equivalence ratio at the burner exit (Z=0) are compared in Figure 9. In the centrifugal case, the (PDF) is distributed across equivalence ratio values ranging from 0.35 to 1.1, indicating a strong inhomogeneity within the mixture. This observation is supported by the sample standard deviation of 0.22. In the centripetal case, although the bounded values are similar, a narrower distribution is observed, characterized by a distinct peak around 0.9 and a smaller standard deviation of 0.16. This suggests a more uniform and homogeneous mixture. While not perfect, this last result is promising.

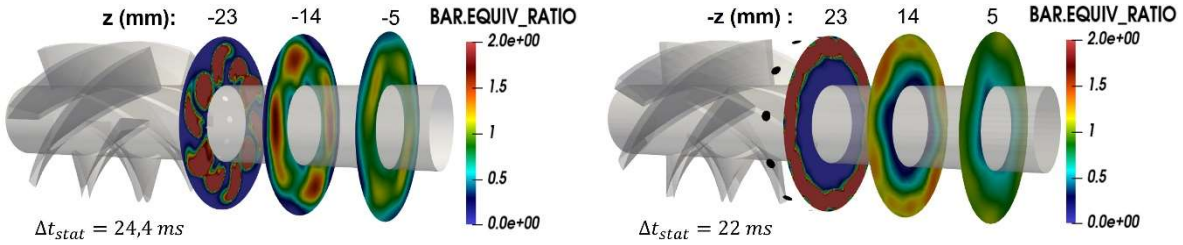

Figure 8. Average equivalence ratio on transverse sections in the burner: (left) centrifugal; (right) centripetal.

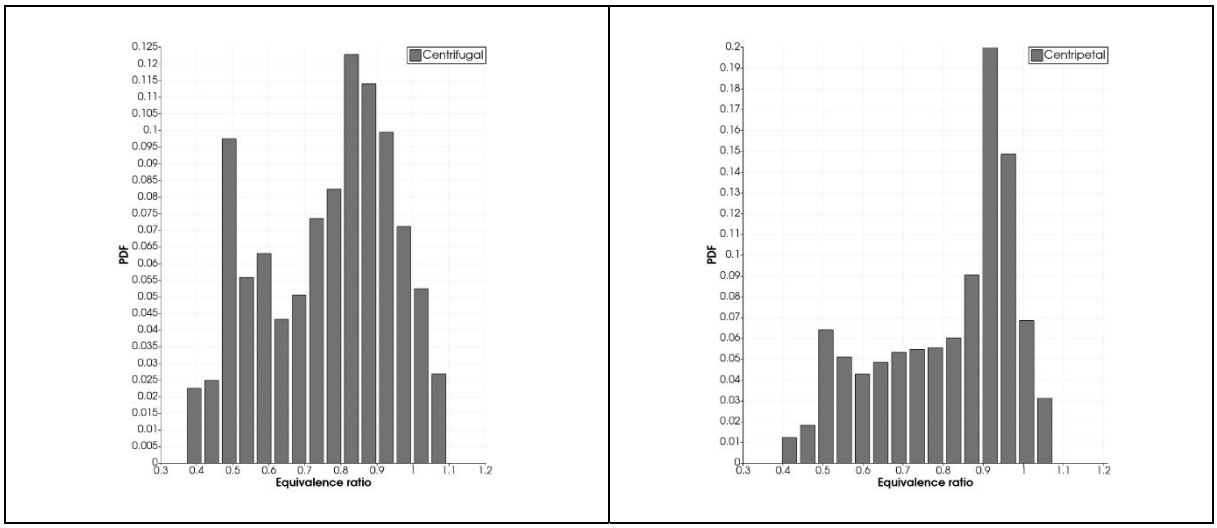

Figure 9. Probability density functions of the equivalence ratio in the injector exit transverse section (z = 0). Left: centrifugal injection; bottom: centripetal injection.

Impact on the flame topology

Figure 10 presents a comparison between average images (symmetry) experimental PLIF-OH and the average numerical OH mass fraction. The simulation shows satisfying agreement with the experimental data, with typical V-shaped flames for centrifugal injection. However, in this injection configuration, Figure 10 shows that the flame tends to anchor on the outer edge of the injector. For centripetal injection, the flame is strongly anchored on both the bluff body and the outer edge of the injector, forming an M-shaped flame. In the centripetal case, higher OH levels are observed towards the outer edge of the injector, while lower levels are found towards the inner edge, which contrasts with the centrifugal injection, as expected. At the chamber base, the centrifugal injector generates a larger amount of heat from the inner side. This is primarily due to the rich hydrogen/air mixture present in the inner recirculation zone. In contrast, the centripetal injector allows for a more homogeneous consumption of hydrogen.

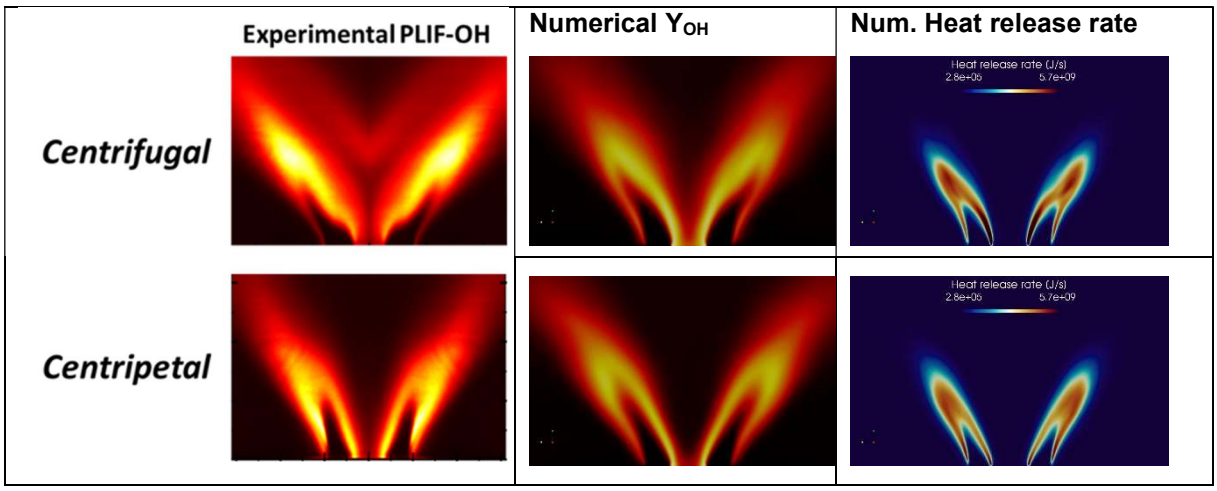

Figure 10. Comparison of the normalised average OH concentrations: (left) PLIF-OH on a half of the plane with its symmetrical counterpart; (right) simulated OH mass fraction.

Impact on NOx emissions

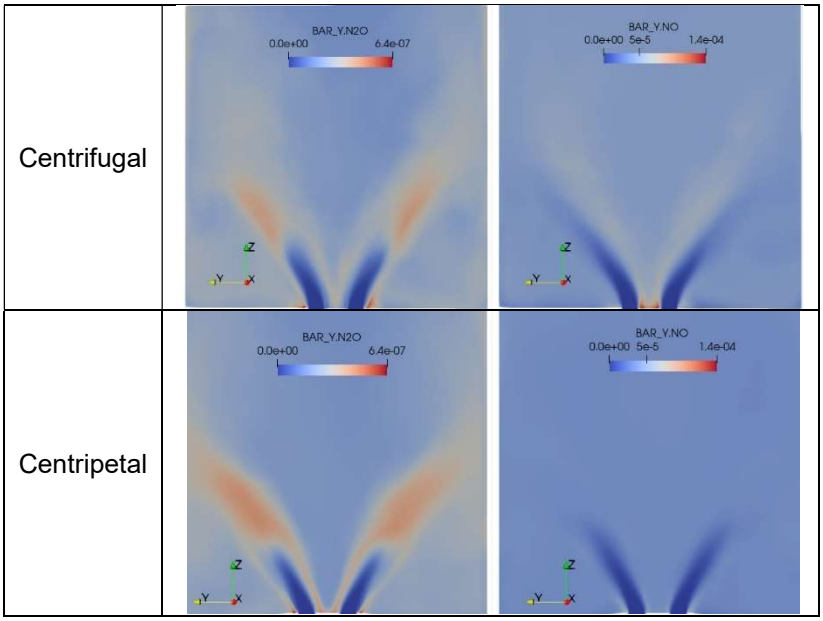

Figure 11. Average fields of N2O et NO resolved mass fractions on a 2D longitudinal cut.

Figure 11 shows the comparison of average NO and N_2O mass fractions between the two injection methods. Qualitatively, the centripetal injector generates less NOx pollutants, especially NO. Quantitative comparisons of Temperature, NO, N_2O and NO_2 on radial profiles at z=0.1 and 0.2 m are provided in Figure 12. It is noteworthy that these profiles are not symmetrical due to a lack of statistical convergence. Indeed, the characteristic chemical time of production of NOx is very high compared to that of hydrogen consumption. However, a clear tendency can be observed. The mass fraction of NO (Figure 12 (b)) is lower by 20% in the centripetal case compared to the centrifugal case. This can be explained by the mean temperature reached by the two injection methods, as shown in Figure 12 (a). The centripetal configuration leads to a reduction of the peak in the mean temperature from 1690 K in the centrifugal case to 1640 K at z = 0.2 m, resulting in reduced NOx emissions.

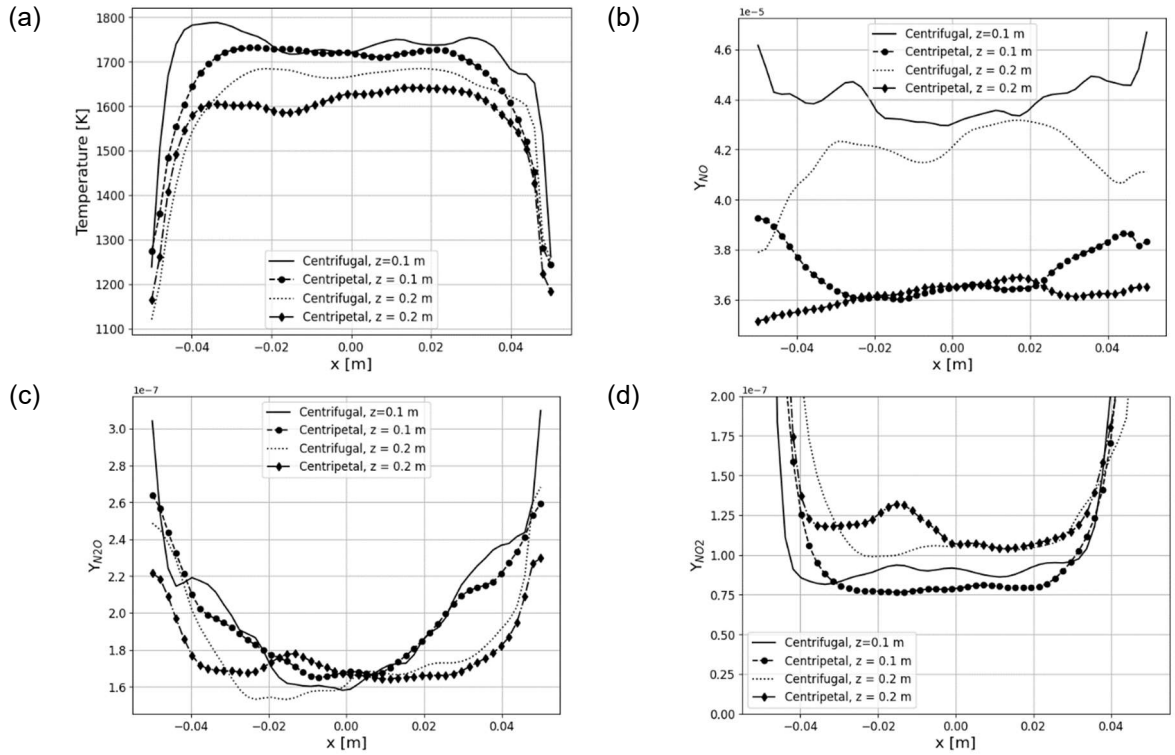

Figure 12. Radial profiles (z = 0.1 and z = 0.2 m) of (a) temperature, (b), NO, (c) NO_2, (d) N_2O mass fractions.

Conclusion

The CORIA HyCoP is a partially premixed burner using both swirl and bluff body stabilization. It is subjected to an extensive investigation using Large Eddy Simulation (LES) and the Thickened Flame Model (TFM) with Adaptive Mesh Refinement (AMR). Following the validation of the LES methodology through a quantitative comparison of velocity fields with experimental data, the current analysis focuses on pure hydrogen combustion. Specifically, it involves a comparative study between a centrifugal injector and a centripetal injector configuration. The latter configuration, where the injection apertures are positioned on the outer tube with higher velocity amplitude, yields a more uniform air/fuel mixture. This adjustment leads to a reduction in the peak of the mean temperature from 1690 K to 1640 K at the end of the square combustion chamber, contributing to lower emissions of NOx pollutants. Both simulations show a good accuracy compared to experimental measurements, with the centripetal case yielding particularly promising results. These simulations reasonably predict the distribution of OH, accurately discerning regions characterized by high and low OH concentrations for each configuration. It is noteworthy that burnt gases above 2000K, constituting here 20% water vapour by mass, is bound to emit radiation. With only water vapor in burnt gases, ambient pressure radiation is unlikely to significantly alter the gas's energy balance or hydrogen combustion (Nmira et al., 2018; Ilbas, 2005), but it is expected to have a substantial impact on the energy balance at the wall. Thermal radiation in diluted hydrogen flames (e.g., with steam or burnt gas recirculation) may affect the laminar flame speed and NOx emissions (Ben Zenou and Vicquelin, 2023). The current study focuses on comparing the relative impact of two injection systems on mixing, flame topology, and NOx emissions. Therefore, LES conclusions and trends remain unaffected by neglecting radiative effects. For a quantitative assessment of its impact, future endeavours will target an in-depth numerical analysis of the combined effects of conjugate heat transfer and thermal radiation on thermal power, wall and gas temperatures, velocity fields and flow/flame dynamics. Furthermore, the experimental database is currently being extended to include the influence of the number and diameter of H_2 injection holes, the mixing length in the premixing chamber, the swirl number and the equivalence ratio. Given the substantial cost associated with designing injection systems, we are also considering the inclusion of additional large-eddy simulations to further enhance and complement the analysis. Finally, the present comprehensive study can provide valuable insight for other burner designs.

Acknowledgment

This work was granted access to the HPC resources of TGCC under allocation Number A0142B10763 from the GENCI (Grand Equipement National de Calcul Intensif) eDARI program.

References

Agostinelli, P.W. *et al.*, On the impact of H2-enrichment on flame structure and combustion dynamics of a lean partially-premixed turbulent swirling flame, *Combust. Flame*, 241, 2022, 112120.

Aniello, A. *et al.*, Experimental and numerical investigation of two flame stabilization regimes observed in a dual swirl H 2 -air coaxial injector, *Combust. Flame*, 249, 2023, 112595.

Baya Toda, H. *et al.*, Assessment of subgrid-scale models with a large-eddy simulation-dedicated experimental database: The pulsatile impinging jet in turbulent cross-flow, *Phys. Fluids*, 26(7), 2014, 075108.

Ben Zenou, J. and Vicquelin, R., Acceleration of premixed H2 -Air-Steam flames when accounting for thermal radiation, *Combust. Flame*, 258, 2023, 113068.

Benard, P., Lartigue, G., Moureau, V., and Mercier, R., Large-Eddy Simulation of the lean-premixed PRECCINSTA burner with wall heat loss, *Proc. Combust. Inst.*, 37(4), 2019, 5233–5243.

Cappelletti, A. and Martelli, F., Investigation of a pure hydrogen fueled gas turbine burner, *Int. J. of Hydrogen Energy*, 42, 2017, 10513-10523.

Charlette, F., Meneveau, C., and Veynante, D., A power-law flame wrinkling model for LES of premixed turbulent combustion Part I: non-dynamic formulation and initial tests, *Combust. Flame*, 131(1-2), 2002, 159–180.

Choi, J. *et al.*, Hydrogen enhancement on a mesoscale swirl stabilized burner array, *Int. J. of Hydrogen Energy*, 46 2021, 23906-23915.

Chterev, I. and Boxx, I., Effect of hydrogen enrichment on the dynamics of a lean technically premixed elevated pressure flame, *Combust. Flame*, 225, 2021, 149-159.

Colin, O., Ducros, F., Veynante, D., and Poinsot, T., A thickened flame model for large eddy simulations of turbulent premixed combustion, *Phys. Fluids*, 12(7), 2000, 1843–1863.

Guiberti, T.F., Durox, D., Zimmer, L., and Schuller, T., Analysis of topology transitions of swirl flames interacting with the combustor side wall, *Combust. Flame*, 162, 2015, 4342-4357.

Ilbas, M., The effect of thermal radiation and radiation models on hydrogen–hydrocarbon combustion modelling, *Int. J. of Hydrogen Energy*, 30, 2005, 1113-1126.

Jaravel, T., Prediction of pollutants in gas turbines using Large Eddy Simulation, Université de Toulouse, 2016.

Legier, J.-P., Poinsot, T., and Veynante, D., Dynamically thickened flame LES model for premixed and non-premixed turbulent combustion, *Proc. of the summer program*, 2000, 157–168.

Marragou, S. *et al.*, Experimental analysis and theoretical lift-off criterion for H2/air flames stabilized on a dual swirl injector, *Proc. of the Combust. Inst.*, 39, 2023a, 4345–4354.

Marragou, S. *et al.*, Modeling of H2/air flame stabilization regime above coaxial dual swirl injectors, *Combust. Flame*, 255, 2023b, 112908.

Mehl, C., Liu, S., and Colin, O., A Strategy to Couple Thickened Flame Model and Adaptive Mesh Refinement for the LES of Turbulent Premixed Combustion, *Flow Turb. Combust*, 107(4), 2021, 1003–1034.

Mehl, C., Liu, S., See, Y.C., and Colin, O., LES of a stratified turbulent burner with a Thickened Flame Model coupled to Adaptive Mesh Refinement and detailed chemistry, *AIAA Joint Propulsion Conference*, 2018.

Nicoud, F. *et al.*, Using singular values to build a subgrid-scale model for large eddy simulations, *Phys. Fluids*, 23(8), 2011, 085106.

Nmira, F., Consalvi, J.-L., and André, F., Pressure effects on radiative heat transfer in hydrogen/air turbulent diffusion flames, *J. Quantitative Spectroscopy and Radiative Transfer*, **220**, 2018, 172-179.

Palulli, R. *et al.*, Characterisation of non-premixed, swirl-stabilised, wet hydrogen/air flame using large eddy simulation, *Fuel*, 350, 2023, 128710.

R. W. Schefer and D. M. Wicksall and A. K. Agrawal, Combustion of hydrogen-enriched methane in a lean premixed swirl-stabilized burner, *Proc. of the Combust. Inst.*, 29, 2002, 843-851.

Richards, Keith J and Senecal, Peter K and Pomraning, Eric, *CONVERGE 3.0*, 2022.

Schmidt, N. *et al.*, Development and characterization of a low-NOx partially premixed hydrogen burner using numerical simulation and flame diagnostics, *Int. J. of Hydrogen Energy*, 48, 2023, 15709-15721.

Schuller, T. *et al.*, Influence of hydrogen content and injection scheme on the describing function of swirled flames, *Combust. Flame*, 240, 2022, 111974.